Remaining useful life prediction of PEMFC systems based on the multi-input echo state network

Zhiguang Hua, Zhixue Zheng, Marie-Cécile Péra, Fei Gao

Version of Record: https://www.sciencedirect.com/science/article/pii/S0306261920303032
Manuscript_007115d8dce5c68d09ed0c4050be628f

Remaining Useful Life Prediction of PEMFC Systems Based on the Multi-input Echo State Network

Zhiguang Hua[1,2], Zhixue Zheng[3], Marie-Cécile Péra[1,2], Fei Gao[1,2]

[1]FEMTO-ST Institute, Univ. Bourgogne Franche-Comté, UTBM, CNRS, Rue Ernest Thierry Mieg, F-90010 Belfort, France.
[2]FCLAB, Univ. Bourgogne Franche-Comté, UTBM, CNRS, Rue Ernest Thierry Mieg, F-90010 Belfort, France.
[3]LMOPS lab, University of Lorraine & CentraleSupélec, 2 Rue Edouard Belin, 57070 Metz, France.
zhiguang.hua@utbm.fr

***Abstract*—The limited durability is one of the key barriers of Proton Exchange Membrane Fuel Cell (PEMFC) to large-scale commercial applications. The data-driven prognostic method aims to estimate the Remaining Useful Life (RUL) without the need for complete knowledge about the system's physical phenomena. As an improved structure of the recurrent neural network, the Echo State Network (ESN) has demonstrated better performances, especially in reducing the computational complexity and accelerating the convergence rate. The traditional prognostic methods utilize only the previous state, e.g. stack voltage, for prediction. Nevertheless, the current operating conditions, such as stack current, stack temperature and the pressures of the reactants (i.e. oxygen and hydrogen) can also contain important degradation information in practice. Especially, the stack current is a crucial operating parameter, since it is normally taken as the scheduling variable and it could reflect the operating conditions. Compared with the single-input and single-output (SISO-ESN) structure, the ESN with multiple inputs and multiple outputs (MIMO-ESN) is proposed in this paper to improve the RUL prediction accuracy. Stack voltage, stack current, stack temperature and the pressures of the reactants are combinedly used to predict the RUL. After the mathematical modeling and the parameter designing, the prediction performance of SISO-ESN and MIMO-ESN are verified and compared on a 1 kW electrical power test bench developed in the laboratory. Results show that the MIMO-ESN method has a better performance than the SISO-ESN method under both static and quasi-dynamic operating conditions.**

***Keywords*—proton exchange membrane fuel cell, prognostics, remaining useful life, data-driven, reservoir computing, echo state network**

I. INTRODUCTION

In recent years, increasingly exhausted conventional fossil fuels and deteriorating environmental are two urgent problems to be solved [1]. With the advantages of high efficiency, non-pollution, and quiet operation, Fuel Cell (FC) is attracting more and more attention and becoming a promising technology to deal with energy and environmental issues [2]. Among all kinds of FC, Proton Exchange Membrane Fuel Cell (PEMFC) system is the most popular one because of its characteristics such as the rapid startup, high power density (3.8~6.5 kW/m^3) and low working temperature (50 ℃~80 ℃) [3]. They are more welcomed in vehicle transportations, portable devices, backup power, and distributed generations [4]. But for many years, durability is one of the key barriers to their large-scale commercialization [5]. The U.S. Department of Energy (DOE) target of durability lifespan is 5,000 h with less than 10 % performance decay in light-duty vehicle transportation applications. Finally, the lifespan target can achieve 8,000 h on a lower average-speed drive cycle by 2020. Nevertheless, the evaluation lifespan in 2015 was 3,900 h before 10 % degradation for the automotive fuel cell systems [6].

Prognostic and Health Management (PHM) has the ability to estimate the future condition based on the past working profiles and the current operations, and then to extend the lifespan based on the Condition-based Maintenance (CBM) [7]. The main objective of prognostic is to predict the Remaining Useful Life (RUL), which is commonly regarded as the time before a certain amount of power loss being reached [8]. Over the last few years, various prognostic methods have been proposed [9]. According to whether an analytical PEMFC model exists, these strategies can be categorized broadly into the model-based, data-driven, and hybrid method [10, 11]. Static or dynamical mathematical models are necessary for the model-based method [12]. The accuracy of prognostic relies on the precision of the degradation models [13]. However, to the best of the authors' knowledge, a general

modeling approach to describe all the degradation mechanisms does not exist yet. It is well to be reminded that the PEMFC is the nonlinear, multi-physics (hydromechanics, electrochemistry, thermodynamics, etc.), and multi-scale (time and space) system [14]. Building up a mathematical model to express the aging phenomenon is difficult, and the degradation mechanisms of FC are not all fully understood. Nonetheless, the model-based method is the simplest method to implement prognostic. In order to retain the prediction accuracy without losing simplicity, some scholars introduced the filtering methods and combined them with the degradation models. This combination is called the hybrid method. In the general hybrid method, the mathematical models are built first, and then different filtering techniques (Unscented Kalman Filter [15], Extend Kalman Filter [16], Particle Filter [17, 18], etc.) are used to realize the RUL prediction. Essentially, the hybrid method also relays on the models of PEMFC.

The data-driven method does not rely on the model of PEMFC. Instead, the historical data of different health indicators are used to realize the RUL prediction. With the development of computer science and the availability of large amounts of operating data, the data-driven method gains popularity over the last several years. As an advanced kernel-based mathematical approach, Relevance Vector Machine (RVM) was use in [19]. Later, the modified RVM was introduced in [20] to improve the accuracy and robustness. Adaptive Neuro Fuzzy Inference Systems (ANFIS) can be regarded as a combination of feed-forward neural network and fuzzy logic system, and this method was used in [21]. The Summation Wavelet-Extreme Learning Machine (SW-ELM) is the combination of single-hidden layer feed-forward neural network and wavelet theory, and it was implemented in [22]. The Long Short-Term Memory (LSTM) recurrent neural network was used in [23] and [24]. Later, the improved structure of grid-LSTM was proposed in [25]. The Recurrent Neural Network (RNN) provides a promising solution to deal with the nonlinearity and temporal problems as it has the inherent ability to memorize the previous state [26]. It has been proved to be a powerful technique to estimate the RUL [27]. Nevertheless, the problems of bifurcations, high computational complexity, and slow convergence rate have limited its practical applications. As a new design and training architecture, the Echo State Network (ESN) which was proposed by Prof. Jaeger et al., has overcome the shortcomings of the traditional RNN [28]. During the implementation of ESN, only the output weight matrix needs to be trained once [29]. As a result, the computational burden is much decreased at the same time while its prediction accuracy is ensured. Together with the Liquid State Machine (LSM) [30] and the Back-Propagation De-Correlation (BPDC) [31], they are three paradigms of Reservoir Computing (RC) [32]. Recently, RC is introduced to realize the diagnostic and prognostic of PEMFC [33]. The RC was used in [34] to realize the fault diagnosis under dynamic load profile and it was also used in [35] to decrease the diagnostic error rate. The ESN was first implemented in [36] to predict the RUL of PEMFC. Both direct and parallel structures with a multi-step prediction were implemented to estimate the RUL. Hereafter, Morando et al. improved their work. Direct structure and iterative structure with one-step ahead prediction are used in [37] and the error rate was 10 % maximum for the RUL estimation of a PEMFC. The Hurst exponent of the signal filtered by wavelet was evaluated in [38]. Compared to [37], better performance with a mean average percentage error of less than 5 % was obtained in [38]. The Multi-reservoir ESN (MR-ESN) was proposed in [39] to increase the prediction accuracy. MR-ESN associated many reservoirs with different spectral radius in parallel. Nevertheless, only the mean cell voltage was used in the papers above, and the load current stayed constant. Lately, Li et al. also did a lot of work on RUL prediction under the various operating conditions and system dynamics [40]. Unlike the traditional health indicators, a virtual steady-state stack voltage was formulated by a series of Linear Parameter Varying (LPV) models identified in the sliding data segments. An ensemble ESN in time-varying model space was implemented in [41] to enhance the adaptability of prognostic and the long-term tests on a low power-scale PEMFC stack in different operating conditions were carried out.

Furthermore, the ESN with single input and single output (SISO-ESN) was used in many papers to predict the RUL of PEMFC. In the SISO-ESN structure, with the previous voltage as the single input and the predicted voltage as the single output. In practice, the ESN has the intrinsic property of dealing with multi-input and multi-output problems. During the implementation of ESN, increasing the inputs improves the dimension of the output weight matrix and the ability to deal with non-linearity issues. The output weight matrix with a high dimension contains more system characteristics and can mimic more accurately the degradation phenomena in the PEMFC system. During the operation of PEMFC, different parameters such as stack current, the temperatures of hydrogen and air, the pressures of hydrogen and air can be easily obtained by the sensors. These parameters can also contain the degradation information of the PEMFC to some extent. Among all the operation parameters, the stack current is the most interesting one because it is normally taken as the scheduling variable. In order to improve the RUL prediction of PEMFC, different operating parameters are investigated together with the stack voltage as the inputs of ESN. As the chosen health indicator of PEMFC, the stack voltage is regarded as the main output of ESN. Other operating parameters can also be predicted at the same time. To the best of the authors' knowledge, the use of ESN

with multiple inputs and multiple outputs (MIMO-ESN) for the RUL prediction is originally explored and studied in this work. This paper is organized as follows. In Section II, mathematical models and design principles of ESN are introduced. Section III presents the experimental platform of the PEMFC system, the analysis of the degradation characteristic, and then the MIMO-ESN implementation process is described. The experiment results are given and further analyzed in Section IV and the conclusions are presented in Section V.

II. ECHO STATE NETWORK

To overcome the weakness of RNN, the structure of the ESN is proposed. The hidden layer of RNN is replaced by a large dynamic "reservoir" which can be excited by suitable inputs. Unlike RNN, the input weight matrix and recurrent weight matrix are not changed once the structure is fixed, and just the output weight matrix is to be optimized by linear regression methods. Therefore, the computation efficiency of ESN is much improved.

A. Mathematical Models

There are three distinct parts of the ESN structure: an input layer, a reservoir, and an output layer. The stack voltage is regarded as a health indicator in this task, and the input layer receives the historical data of stack voltage, temperature, pressure, etc. In general, the more neurons are used in the reservoir, the less difficulty exists in the liner separation. Finally, the expected output is optimized via a multi-linear regression. The general structure of the ESN is illustrated in Fig. 1.

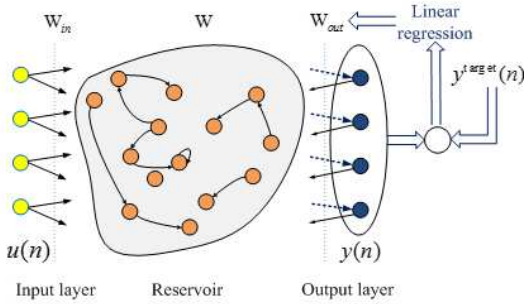

Fig. 1. The structure of Echo State Network

In discretized time, the typical model of ESN can be represented as

$$\tilde{\mathbf{x}}(n) = f(\mathbf{W}_{in}\mathbf{u}(n) + \mathbf{W}\mathbf{x}(n-1)) \qquad (1)$$

$$\mathbf{x}(n) = (1-\alpha)\mathbf{x}(n-1) + \alpha\tilde{\mathbf{x}}(n) \qquad (2)$$

Where $f(\cdot)$ is the nonlinear neuron activation function and $\tanh(\cdot)$ is commonly used, $\alpha \in (0,1]$ is the leakage rate, $\mathbf{u}(n) \in \mathbf{R}^{N_u}$ is the input vector, $\mathbf{x}(n) \in \mathbf{R}^{N_x}$ is the vector of reservoir neuron activation and $\tilde{\mathbf{x}}(n) \in \mathbf{R}^{N_x}$ is its update at time step n, $\mathbf{W}_{in} \in \mathbf{R}^{N_x \times N_u}$ and $\mathbf{W} \in \mathbf{R}^{N_x \times N_x}$ are respectively the input weight matrix and recurrent weight matrix. When the ESN has K inputs, N reservoir neurons, and L outputs, the $\mathbf{u}(n)$ and $\mathbf{x}(n)$ can be expressed as

$$\mathbf{u}(n) = (\mathbf{u}_1(n), \ldots, \mathbf{u}_K(n)), \quad n = 1, \ldots, T \qquad (3)$$

$$\mathbf{x}(n) = (\mathbf{x}_1(n), \ldots, \mathbf{x}_N(n)), \quad n = 1, \ldots, T \qquad (4)$$

The linear readout layer of ESN is defined as

$$\mathbf{y}(n) = \mathbf{W}_{out}[\mathbf{u}(n); \mathbf{x}(n)] \qquad (5)$$

Where $\mathbf{y}(n) \in \mathbf{R}^{N_y}$ is the output vector, $\mathbf{W}_{out} \in \mathbf{R}^{N_y \times (N_u + N_x)}$ is the output weight matrix, and $[;]$ stands for a vertical vector concatenation. The $\mathbf{y}(n)$ can be expressed as

$$\mathbf{y}(n) = (\mathbf{y}_1(n), \ldots, \mathbf{y}_L(n)), \quad n = 1, \ldots, T \qquad (6)$$

The $\mathbf{W}_{out}$ can be calculated by minimizing the Root Mean Square Error (RMSE) between the predicted value $\mathbf{y}(n)$ and the target value $\mathbf{y}^{\text{target}}(n)$.

$$\mathbf{W}_{out} = \arg\min \sqrt{\frac{1}{m}\sum_{i=1}^{m}(\mathbf{y}_i(n) - \mathbf{y}_i^{\text{target}}(n))^2} \qquad (7)$$

Where m is the number of data points in the training data set. Ridge regression is the most universal and stable way to calculate the output weight matrix.

$$\mathbf{W}_{out}=\mathbf{Y}^{\text{target}}\mathbf{X}^{\mathrm{T}}(\mathbf{X}\mathbf{X}^{\mathrm{T}}+\beta\mathbf{I})^{-1} \quad (8)$$

Where $\mathbf{x}$ represents the output of the reservoir, $\mathbf{Y}^{\text{target}}$ is the target output signal, β is the regularization parameter, and $\mathbf{I}$ is the identity matrix.

B. Designing Principles

The parameters in ESN can be divided into three groups: assigned parameters, adjustable parameters, and calculated parameters. The assigned parameters include the input weight matrix $\mathbf{W}_{in}$, recurrent weight matrix $\mathbf{W}$, input units K, and output units L. Gaussian distributions, symmetrical uniform, and normal distribution centered around zero are commonly used principles to generated the input and recurrent weight matrix. These two matrices are assumed to be fixed once they are generated randomly. The adjustable parameters include the spectral radius ρ, the leakage rate α, and the number of reservoir neurons N_{res}. The spectral radium is the maximal absolute eigenvalue of the matrix $\mathbf{W}$. It is an important parameter that controls the dynamic regime of the reservoir. To ensure the echo state property, the spectral radius is always less than 1 for zero inputs. Nevertheless, for nonzero inputs, the system usually has better performance when the spectral radius is bigger than 1 in practice [42]. The leakage rate represents the update speed of the neurons in the reservoir. The dynamic of the reservoir increases with the value of leakage rate, and a large value of leakage rate means that the output value of the reservoir at time step (t-1) has little impact on the reservoir state at time step (t). Generally speaking, when the reservoir includes more neurons, the performance would be better. It is easier to find a linear combination of the inputs to target outputs when the dimension of the reservoir increases. However, the computation time would increase at the same time. The selection of reservoir neurons is to find a tradeoff between the prediction accuracy and the computation complex. The regularization parameter is set manually. The calculated parameter is the output weight matrix $\mathbf{W}_{out}$, and it can be calculated by the multi-linear regression.

According to the above designing rules, the ESN for predicting the RUL of PEMFC is developed. The parameters of ESN are determined after several repeated attempts to implement the RUL estimation. Implementation framework of the proposed ESN and some parameters are shown in Fig. 2 and Table Ⅰ.

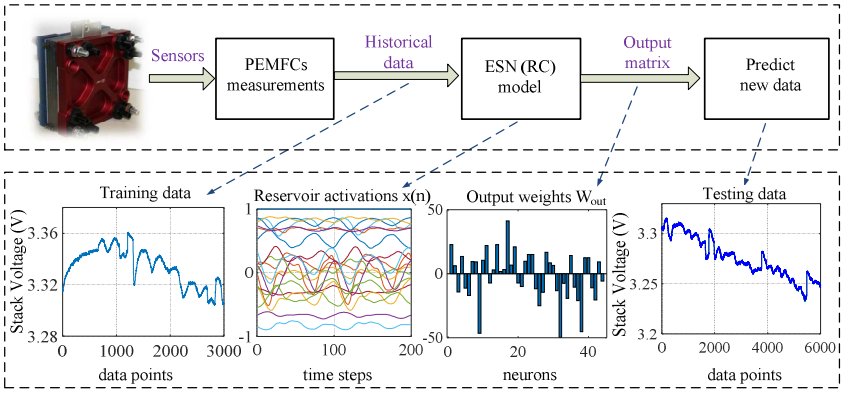

Fig. 2. Implementation framework of the ESN method

TABLE Ⅰ. KEY PARAMETERS OF ESN

Parameter	Values
reservoir neurons N_{res}	400
leakage rate α	[0.3, 0.5]
spectral radius ρ	[0.4, 1.0]
regularization parameter β	8×10^{-2}
input weight matrix $\mathbf{W}_{in}$	[-0.5, 0.5]
recurrent weight matrix $\mathbf{W}$	[-0.5, 0.5]

III. AGING EXPERIMENTAL IMPLEMENTATION

A. *Experimental Platform*

The experiment is applied to the data of PEMFC from the IEEE PHM 2014 Data Challenge [8]. The PEMFC platform which is adapted for 1 kW electrical power was built for the experiment. This test bench has 5 cells, and each cell has an active area of 100 cm^2. The nominal current density of the stack is 0.7 A/cm^2, and the maximal current density is 1.0 A/cm^2. Hydrogen loop and air loop are two reactant loops of the test bench. Two independent boilers (air and hydrogen boilers) are placed upstream of the stack to realize the reactant humidification. The air boiler is heated in order to get the desired relative humidity of the air, and the hydrogen boiler remains at room temperature. The supplication rate of reactants is adjusted by the pressure and flow valves in order to avoid the FC stack "starvation" [43]. The temperature of the stack is controlled by a cooling water system. Moreover, the FC stack enables normal and accelerated aging tests under constant and dynamic operating conditions. The physical parameters in the test bench can be measured and controlled in order to manage the PEMFC operating conditions as accurately as possible. Health monitoring data like the voltage, current, pressure, temperature, etc. are monitored by different sensors. Some of the controllable and operating parameters are presented in Table Ⅱ, and the test bench is shown in Fig. 3.

TABLE Ⅱ. PHYSICAL AND OPERATING PARAMETERS OF THE TEST BENCH

Parameter	Control range
Temperature	20 ℃~ 80 ℃
Cooling flow	0~10 L/min
Gas temperature	20 ℃~ 80 ℃
Gas humidification	0~100 % RH
Air flow	0~100 L/min
H_2 flow	0~30 L/min
Gas pressure	0~2 Bar
Fuel current	0~300 A
$T_{in}H_2$; $T_{out}H_2$	Inlet/Outlet temperatures of H_2 (℃)
T_{in}Air ; T_{out}Air	Inlet/Outlet temperatures of air (℃)
T_{in}Wat ; T_{out}Wat	Inlet/Outlet temperatures of water (℃)
$P_{in}H_2$; $P_{out}H_2$	Inlet/Outlet pressure of H_2 (mBar)
P_{in}Air ; P_{out}Air	Inlet/Outlet pressure of air (mBar)

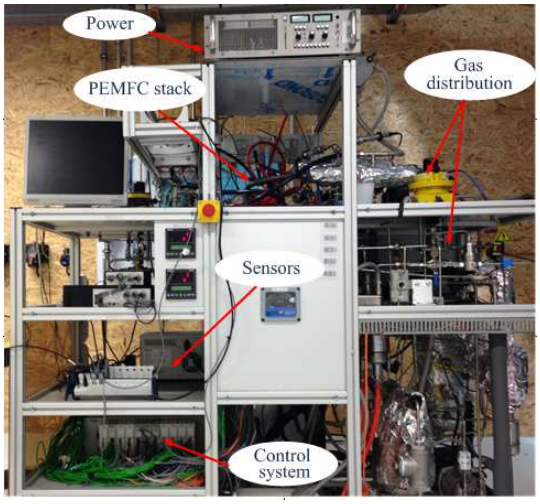

Fig. 3. The 1 kW test bench of PEMFC system developed in the laboratory

B. *Characteristic Analysis*

Two long-term durability tests for more than 1,000 h were implemented: the first test was operated under a static current operating condition (FC1), and the second test was operated under a quasi-dynamic current operating condition (FC2) [44]. The constant load current of 70 A is imposed to the aging test of FC1. In the aging test of

FC2, a triangular ripple current of 7 A with 5 kHz is superimposed to the constant current of 70 A. The durability tests of different load currents are shown in Fig. 4. The Electrochemical Impedance Spectroscopy (EIS) test and polarization curve measurements were implemented in the test bench to analyze the quasi-dynamic and static properties of the PEMFC. Polarization curves of the single cells and stack were measured under a current ramp from 0 A/cm^2 to 1 A/cm^2 during 1000 s. The polarization curves of the two tests are shown in Fig. 5. They show that the stack voltage decreases with the increase of the stack current at each duration time. At the same duration time (e.g., 515 h), the degradation is more serious under the quasi-dynamic current operating conditions (from P to Q in Fig. 5). In general, the longer the duration time is, the more serious the stack degradation is. More properly, the single-cell and stack voltage decrease as time grows, which depicts the degradation phenomena of the test bench. In the PEMFC system, the stack voltage sensors are easy for installation and implementation, and the voltage is always supervised for control purposes. For convenience, the stack output voltage is also widely accepted as a health indicator of PEMFC systems. Nevertheless, the raw data contain lots of disturbance noise and large peaks, which would have an effect on the RUL prediction. Before using this data to predict the RUL, the Moving Average Filtering (MAF) method is applied here to remove the peaks and noise.

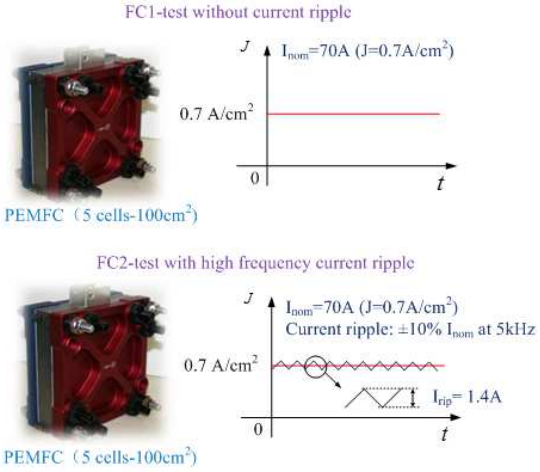

Fig. 4. Durability tests of FC1 and FC2

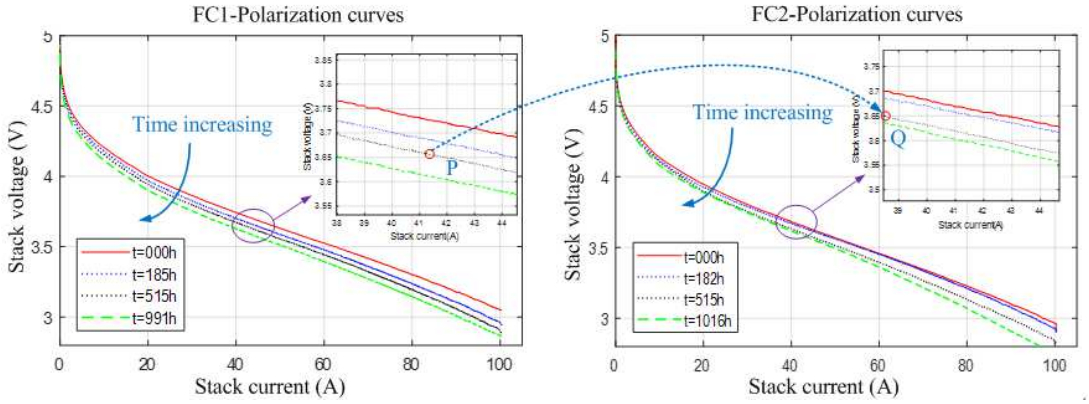

Fig. 5. Polarization curves of FC1 and FC2

C. *Implementation of the MIMO-ESN*

During the fuel cell running, many operating parameters are supervised to guide a more durable working lifespan. The operating parameters of FC1 and FC2 are shown in Fig. 6 and Fig. 7. The characteristics of all the parameters are shown in Table Ⅲ. Signal-to-Noise Ratio (SNR) is used to measure the quality of parameters, and it can be expressed as

$$\mathrm{SNR}=10*\log_{10}(Ps/Pn) \qquad (9)$$

Where Ps is the power of the signal and Pn is the power of the noise. Among all the parameters, the stack current (I_s) has the highest SNR both in FC1 and FC2. In this paper, MIMO-ESN is defined as

Single-input ESN: the input is the stack voltage (U_s).

Two-input ESN: the inputs are the combination of U_s and one of the parameters in Table Ⅲ.
Three-input ESN: the combination of U_s and two of the parameters in Table Ⅲ.
So, there are $C_{11}^1 = 11$ combinations in 2-input ESN, and $C_{11}^2 = 55$ combinations in 3-input ESN.

TABLE Ⅲ. THE SIGNAL-TO-NOISE RATIO OF FC

Parameter	characteristics	SNR of FC1(dB)	SNR of FC2(dB)
I_s	Regulated (A)	78.72	70.33
$T_{in}H_2$	Measured (°C)	65.51	62.85
$T_{out}H_2$	Measured (°C)	45.58	43.06
$T_{in}Air$	Measured (°C)	55.25	52.32
$T_{out}Air$	Measured (°C)	61.42	57.18
$T_{in}Wat$	Regulated (°C)	55.39	52.65
$T_{out}Wat$	Regulated (°C)	59.42	56.12
$P_{in}Air$	Measured (mBar)	58.83	58.84
$P_{out}Air$	Regulated (mBar)	59.39	58.79
$P_{in}H_2$	Regulated (mBar)	50.93	51.57
$P_{out}H_2$	Regulated (mBar)	51.31	52.02

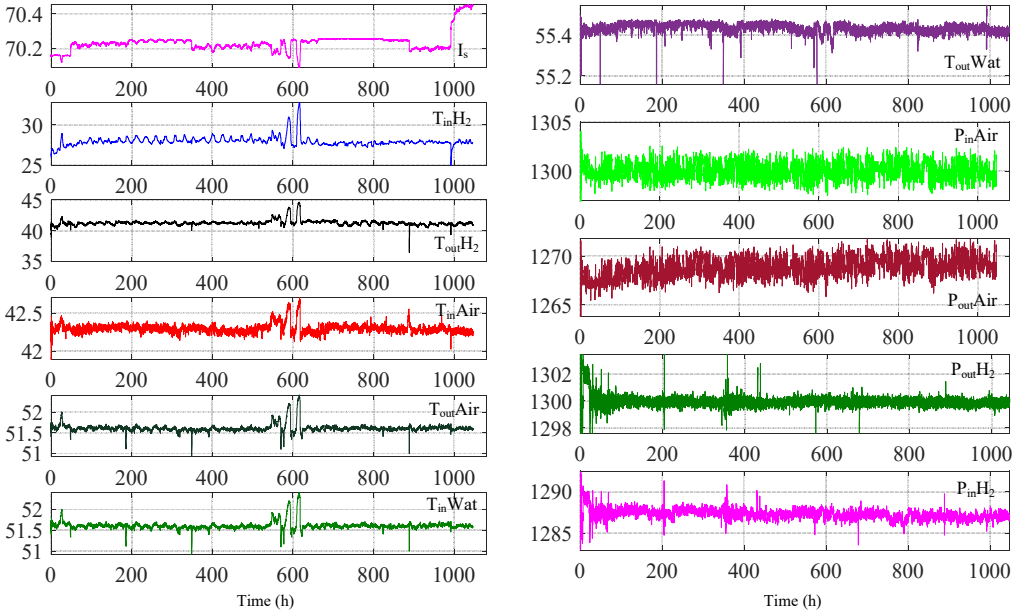

Fig. 6. Operating parameters of FC1

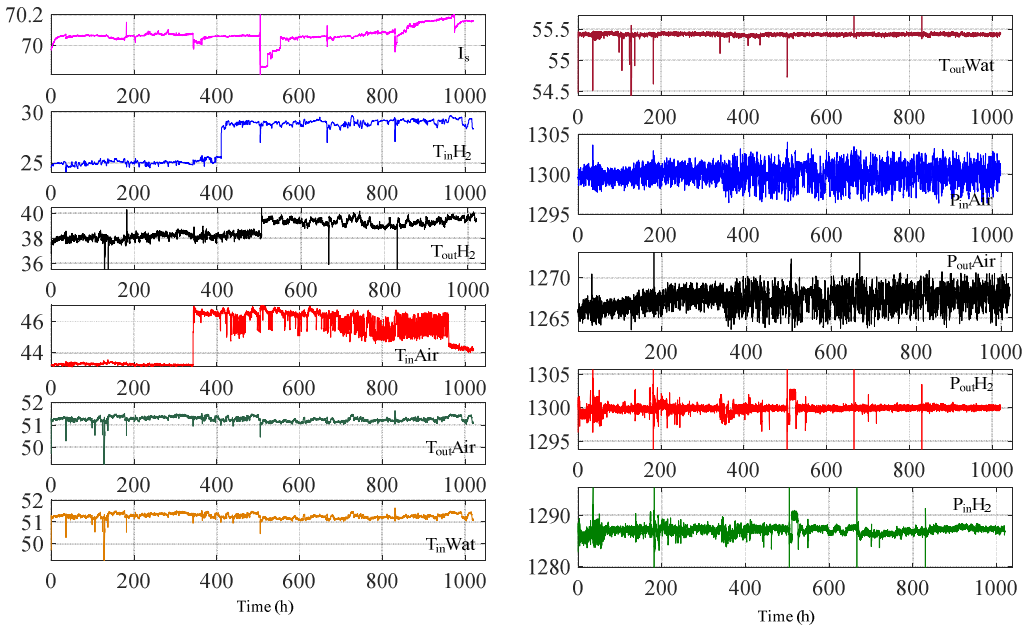

Fig. 7. Operating parameters of FC2

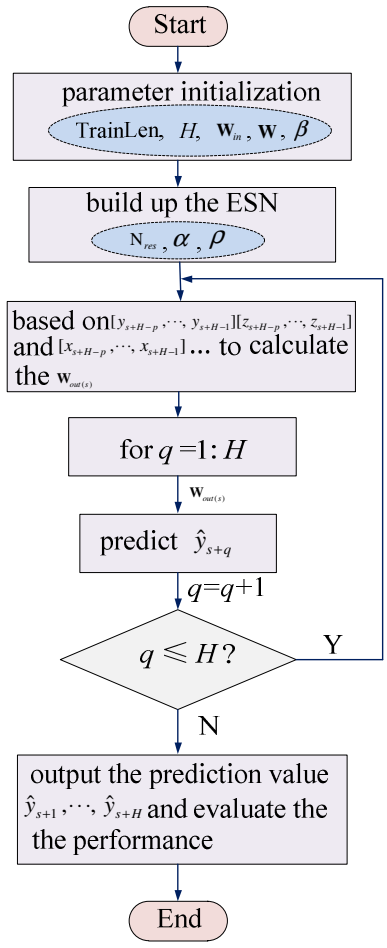

Fig. 8. Calculation flow chart of the MIMO-ESN prediction process

The calculation flow chart of the MIMO-ESN method is shown in Fig. 8, where H denotes the final prediction points, p is the number of past discrete values used for prediction and q is the prediction steps.

For single-input ESN, an iterative one-step prediction method is utilized for the multi-step prediction. The sampling points of the stack voltage (U_s) can be expressed as $\{(t_1, y_1), \ldots, (t_i, y_i), \ldots, (t_M, y_M)\}$, where t_i represents the sampling time, y_i represents the stack voltage at time t_i, and index M denotes the total number of data points. The

time interval of each two points is 30 minutes. Firstly, the sampling points $\{(t_1, y_1), ..., (t_s, y_s)\}$ are trained to calculate the output weight matrix $\mathbf{W}_{out(s)}$. Once $\mathbf{W}_{out(s)}$ is obtained during the training process, it is fixed. Then based on $\mathbf{W}_{out(s)}$ and y_s, the voltage value of the next step is predicted as $\hat{y}_{s+1}$. When the system reaches time t_{s+1}, $\hat{y}_{s+1}$ and $\mathbf{W}_{out(s)}$ are used to predict the $\hat{y}_{s+2}$. The same sequence is repeated for $\hat{y}_{s+3}$, $\hat{y}_{s+4}$ … etc.

For multi-input ESN, besides the one-step iterative prediction method for stack voltage, a one-step ahead prediction method is applied to the operating parameters. Taking the double inputs stack voltage (U_s) and stack current (I_s) for example, the sampling data points can be expressed as $\{(t_1, y_1), ..., (t_i, y_i), ..., (t_M, y_M)\}$ and $\{(t_1, z_1), ..., (t_i, z_i), ..., (t_M, z_M)\}$. Where z_i represents the stack current at the time t_i. Firstly, the sampling points $\{(t_1, y_1), ..., (t_s, y_s)\}$ and $\{(t_1, z_1), ..., (t_s, z_s)\}$ are trained to calculate the output weight matrix $\mathbf{W}_{out(s)}$. Then based on $\mathbf{W}_{out(s)}$, y_s and z_s, the voltage value of the next step is predicted as $\hat{y}_{s+1}$ and $\hat{z}_{s+1}$. After that, $\hat{y}_{s+1}$, z_{s+1} and $\mathbf{W}_{out(s)}$ are used to predict the $\hat{y}_{s+2}$ and $\hat{z}_{s+2}$. The same sequence is repeated for $\hat{y}_{s+3}$, $\hat{y}_{s+4}$ … etc. It should be taken attention that the operating parameters such as stack current are usually scheduling variables and cannot be predicted in the same iterative way as the stack voltage. A major potential assumption herein is that the operating parameters can be schedulable or programmable such as in the homemade test benches and Combined Heat and Power (CHP) applications.

Based on the MIMO-ESN, the stack voltage is not only dependent on the historical profile but also related to the operating conditions. Finally, the prediction voltages and the actual voltages are compared to evaluate the prediction performance. In the practical application, the output weight matrix W_{out} is firstly calculated offline, then the stack voltage at time step (t) and the W_{out} are used to predict the new value at the time step (t+1). The computing time during the prediction process is about 20 seconds (Matlab 2018a, 8G RAM, Core i5-2450 CPU @ 2.50 GHz) in this paper and it is short enough for the several hundred hours' lifespan prediction. The block diagram of single-input and multi-input ESN is shown in Fig. 9.

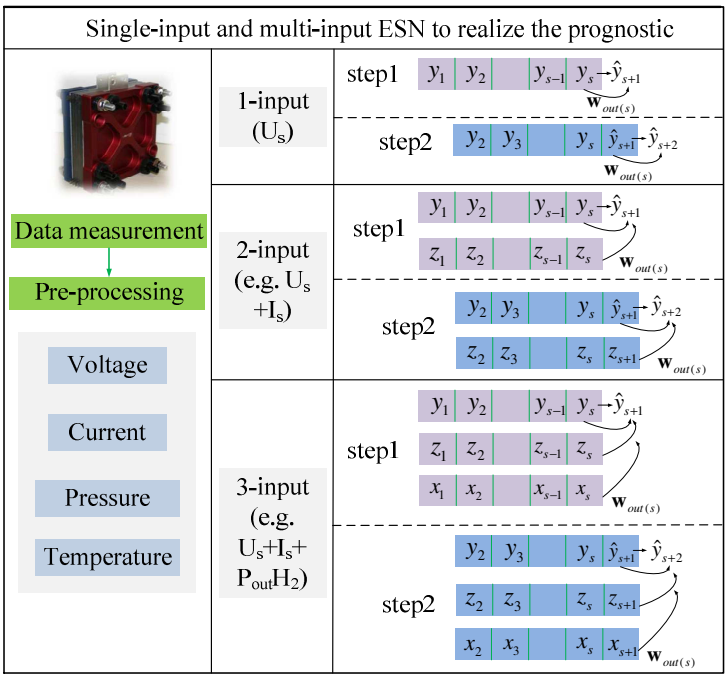

Fig. 9. Block diagram of single-input and multi-input ESN for one example with 2 steps in each case (where y_i represents U_s at time t_i, z_i represents the I_s at time t_i, x_i represents $P_{out}H_2$ at time t_i, $\hat{y}_{s+1}$ and $\hat{y}_{s+2}$ are next-step predicted stack voltage value, $\mathbf{W}_{out(s)}$ represents the output weight matrix)

IV. Experimental Results

A. *Criteria of Prediction Accuracy*

In the experiments of FC1 and FC2, the RUL is regarded as the time before a certain amount of voltage loss is reached. More precisely, 3.0 %, 3.5 %, 4.0 %, 4.5 %, and 5.0% of initial voltage (V_{init} = 3.35 V) are considered to be the failure thresholds (FT) of FC1. The stack voltage under the quasi-dynamic condition decreases more seriously than that under the static condition. Similar with the static operation, the 3.5 %, 4.0 %, 4.5 %, 5.0 % and

5.5 % of initial voltage (V_{init} = 3.33 V) are considered to be the FT of FC2. The first intersection of the filtered voltage and FT is regarded as the failure point.

Three quantitative metrics are used to evaluate the prediction performance: 1) Root Mean Square Error (RMSE) which is commonly used to quantify the difference between the real signal ($\mathbf{y}_i^{\text{target}}(n)$) and its forecasted value ($\mathbf{y}_i(n)$) during the RUL time (m data points), 2) Mean Average Percentage Error (MAPE), which is also a quantification measurement between two signals, and 3) the percentage error ($\%\text{Er}_{\text{FT}}$) between the actual RUL (t_{RUL}^{act}) and the prediction one (t_{RUL}^{pre}) which is also defined to evaluate the accuracy of ESN.

$$\text{RMSE} = \sqrt{\frac{1}{m}\sum_{i=1}^{m}(\mathbf{y}_i(n) - \mathbf{y}_i^{\text{target}}(n))^2} \tag{10}$$

$$\text{MAPE} = \frac{1}{m}\sum_{i=1}^{m}\left|\frac{\mathbf{y}_i(n) - \mathbf{y}_i^{\text{target}}(n)}{\mathbf{y}_i(n)}\right| \tag{11}$$

$$\%\text{Er}_{\text{FT}} = \frac{t_{RUL}^{act} - t_{RUL}^{pre}}{t_{RUL}^{act}} \times 100 \tag{12}$$

Regarding the RUL estimation, there are two cases: 1) the estimation is smaller than the actual RUL, it is an early prediction, or 2) the estimation is greater, it is a late prediction. In practical, good performance of estimations relates to early predictions of RUL (i.e. cases where $\%\text{Er}_{\text{FT}} > 0$), with a deduction to early removal, and more severe deductions for RUL estimates that exceed actual RUL (i.e. cases where $\%\text{Er}_{\text{FT}} < 0$).

B. Prognostic under Static Operation

In the static operation task, the data that are used for the experiment come from a 1050 h duration test on the PEMFC stack. The data between 0 h and $t_{predict}$ are used for training, and the rest of the data are used for the prediction. The RUL time (t_{RUL}) can be considered as the time between the prediction time ($t_{predict}$) and the failure time ($t_{failure}$). For FC1, the actual values at different FT are 95.8 h (3.0 %), 127.1 h (3.5 %), 277.6 h (4.0 %), 284.1 h (4.5 %), and 354.5 h (5.0 %) respectively. In the static operation, the data from 0 h to 550 h are applied to training, and the data from 550 h to 1050 h are used for the prediction. The RUL prediction of FC1 based on single-input (U_s) ESN is shown in Fig. 10.

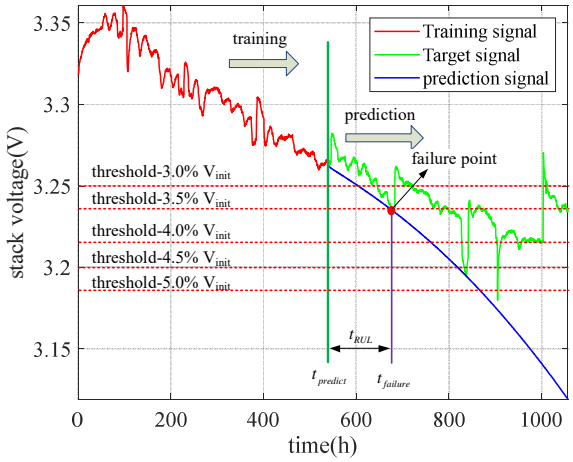

Fig. 10. The RUL prediction of FC1 based on single-input ESN

With all the other parameters remaining unchanged, the number of inputs is increased to test the prediction performance. The RUL predictions of FC1 based on 2-input ESN are shown in Fig. 11 and the prediction results of 4 combinations at different failure thresholds are given in Table Ⅳ. The RMSE and MAPE of 2-input ESNs are lower than single-input ESN. Results represent that the prediction accuracy of 2-input ("U_s+T_{out}Air", "U_s+I_s", "U_s+T_{in}Wat", "U_s+$P_{out}H_2$") ESN is higher than single-input ESN. It also means that 2-input data are more sufficient to mimic the degradation characteristics, and the prediction accuracy is improved by increasing another input to the ESN.

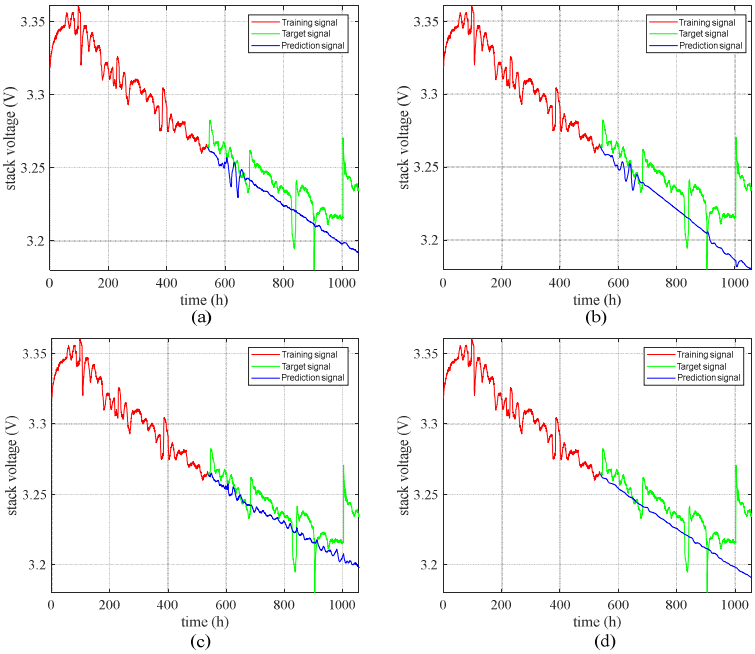

Fig. 11. The RUL prediction of FC1 based on 2-input ESN: (a) stack voltage (U_s) and outlet temperature of air ($T_{out}Air$). (b) stack voltage (U_s) and stack current (I_s). (c) stack voltage (U_s) and inlet temperature of water ($T_{in}Wat$). (d) stack voltage (U_s) and outlet pressure of H_2 ($P_{out}H_2$).

TABLE Ⅳ. PREDICTION RESULTS OF FC1 BASED ON 2-INPUT ESN

inputs	Prediction values (h)	%Er_{FT}	RMSE	MAPE
U_s	54.2	43.4	0.01188	0.00343
	136.8	-7.6	0.01077	0.00300
	208.5	24.9	0.02039	0.00560
	272.3	4.2	0.02018	0.00551
	329.5	7.1	0.02710	0.00709
U_s+ $T_{out}Air$	45.5	52.51	0.01281	0.00341
	91.5	28.01	0.01146	0.00289
	320.0	-15.27	0.01190	0.00330
	441.2	-55.30	0.01211	0.00336
	500.0	-41.04	0.01339	0.00375
U_s+I_s	48.7	49.16	0.01143	0.00312
	175.5	-38.08	0.01048	0.00275
	281.8	-1.51	0.01295	0.00365
	366.5	-29.00	0.01297	0.00367
	456.0	-28.63	0.01532	0.00429
U_s+ $T_{in}Wat$	59.6	37.79	0.00902	0.00242
	209.3	-64.67	0.00808	0.00205
	344.6	-24.14	0.00931	0.00249
	500.0	-75.99	0.00972	0.00258
	500.0	-41.04	0.01106	0.00295
U_s+ $P_{out}H_2$	77.0	19.62	0.00910	0.00245
	194.7	-53.19	0.00815	0.00207
	310.0	-11.67	0.01017	0.00281
	431.6	-51.92	0.01045	0.00288
	500.0	-41.04	0.01236	0.00339

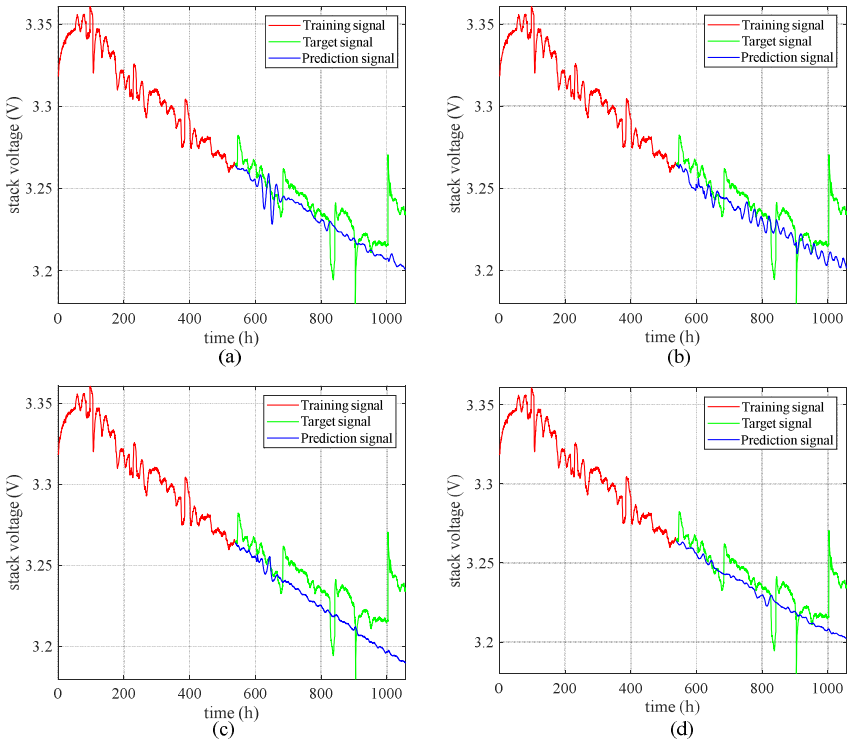

Fig. 12. The RUL prediction of FC1 based on 3-input ESN: (a) stack voltage (U_s), inlet temperature of H_2 ($T_{in}H_2$) and inlet pressure of H_2 ($P_{in}H_2$). (b) stack voltage (U_s), outlet temperature of H_2 ($T_{out}H_2$) and outlet temperature of air ($T_{out}Air$). (c) stack voltage (U_s), inlet temperature of air ($T_{in}Air$) and outlet temperature of water ($T_{out}Wat$). (d) stack voltage (U_s), outlet pressure of H_2 ($P_{out}H_2$), and inlet pressure of H_2 ($P_{in}H_2$).

TABLE Ⅴ. PREDICTION RESULTS OF FC1 BASED ON 3-INPUT ESN

inputs	Prediction values (h)	%Er_{FT}	RMSE	MAPE
U_s +$T_{in}H_2$ +$P_{in}H_2$	71.6	25.26	0.00937	0.00239
	98.2	22.74	0.00930	0.00239
	358.5	-29.14	0.00850	0.00226
	500.0	-75.99	0.00930	0.00239
	500.0	-41.04	0.01051	0.00271
U_s +$T_{out}H_2$ +$T_{out}Air$	41.5	56.68	0.01047	0.00284
	186.8	-46.97	0.00956	0.00252
	347.5	-25.18	0.00959	0.00258
	500.0	-75.99	0.01001	0.00267
	500.0	-41.04	0.01075	0.00287
U_s +$T_{out}Wat$ +$T_{in}Air$	73.2	23.59	0.00904	0.00236
	188.4	-48.23	0.00817	0.00207
	307.4	-10.73	0.01061	0.00293
	436.8	-53.75	0.01080	0.00298
	500.0	-41.04	0.01266	0.00349
U_s +$P_{out}H_2$ +$P_{in}H_2$	81.2	15.24	0.00789	0.00199
	226.1	-77.89	0.00722	0.00177
	370.3	-33.39	0.00819	0.00219
	500.0	-75.99	0.00898	0.00232
	500.0	-41.04	0.01027	0.00265

Furthermore, more parameters are regarded as the inputs of ESN to investigate its prediction performance. The RUL predictions of FC1 based on 3-input ESN is shown in Fig. 12. The prediction results of 3-input ESN at different failure thresholds are given in Table Ⅴ. Results represent that some of the 3-input ESN ("U_s+$T_{in}H_2$+$P_{in}H_2$" and "U_s+$T_{out}H_2$+T_{out}Air") have a better prediction performance than 2-input ESN. Sometimes, they are worse than 2-input ESN ("U_s+T_{in}Air+T_{out}Wat" and "U_s+$P_{out}H_2$+$P_{in}H_2$").

C. Prognostic under Quasi-Dynamic Operation

In the quasi-dynamic operation task, the data set come from a 1020 h duration test on the PEMFC. For FC2, the actual values at different FT are 21.4 h (3.5 %), 194.2 h (4.0 %), 209.7 h (4.5 %), 384.3 h (5.0 %), and 386.7 h (5.5 %) respectively. The data from 0 h to 550 h are applied to training, and the data from 550 h to 1020 h are used for prediction. The RUL prediction of FC2 based on single input ESN is shown in Fig. 13. The RUL prediction of FC2 based on 2-input ESN is shown in Fig. 14 and the prediction results of 4 combinations at different failure thresholds are given in Table Ⅵ. The RMSE and MAPE of 2-input ESN are lower than the single-input one. Under the quasi-dynamic condition, the prediction results of 2-input ("U_s+T_{out}Air", "U_s+I_s", "U_s+T_{in}Wat", and "U_s+$P_{out}H_2$") ESN perform better than single-input ESN. They also represent that the prediction accuracy is improved by increasing the number of inputs. The prediction error of FC2 is bigger than FC1 when the training length (0~550 h) is the same. Because of the prediction processes of FC2 have more perturbations (two faults in Fig. 13) than FC1. The results also mean that the ESN structure has more difficulties to mimic the quasi-dynamic operation when compared with the static operation. The RUL predictions of FC2 based on 3-input ESN are shown in Fig. 15. The prediction results of 3-input ESN at different failure thresholds are given in Table Ⅶ. Results represent that some of the 3-input ESN ("U_s+T_{in}Wat+$P_{in}H_2$" and "U_s+P_{out}Air+T_{in}Air") have a better prediction performance than 2-input ESN. Sometimes, they are worse than 2-input ESN ("U_s+$T_{in}H_2$+$P_{in}H_2$" and "U_s+$T_{out}H_2$+T_{out}Air").

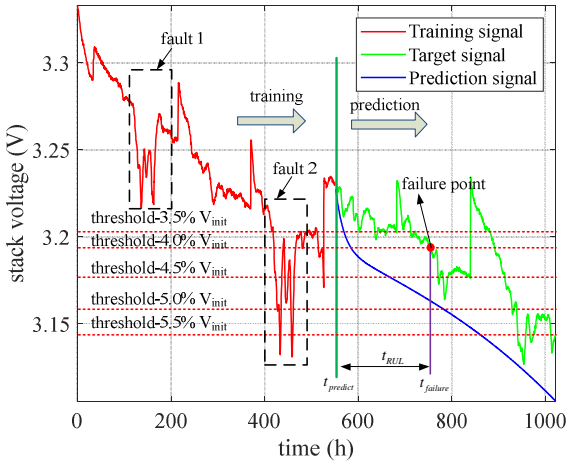

Fig. 13. The RUL prediction of FC2 based on single-input ESN

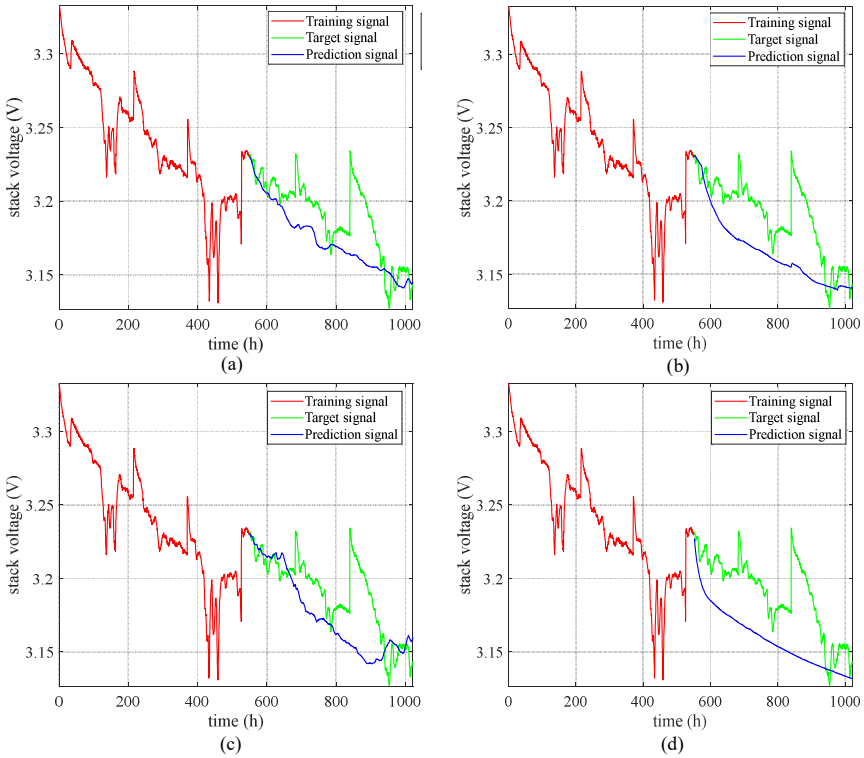

Fig. 14. The RUL prediction of FC2 based on 2-input ESN: (a) stack voltage (U_s) and outlet temperature of air ($T_{out}Air$). (b) stack voltage (U_s) and stack current (I_s). (c) stack voltage (U_s) and inlet temperature of water ($T_{in}Wat$). (d) stack voltage (U_s) and outlet pressure of H_2 ($P_{out}H_2$).

TABLE Ⅵ. PREDICTION RESULTS OF FC2 BASED ON 2-INPUT ESN

inputs	Prediction values (h)	%Er_{FT}	RMSE	MAPE
U_s	12.5	41.6	0.01839	0.00520
	36.0	81.5	0.02915	0.00868
	122.5	41.6	0.02900	0.00866
	222.8	42.0	0.03811	0.01082
	314.2	18.7	0.03789	0.01078
U_s+ $T_{out}Air$	34.8	-62.62	0.00652	0.00154
	100.2	48.40	0.01864	0.00484
	189.1	9.82	0.01878	0.00495
	322.2	16.16	0.02532	0.00640
	428.5	-10.81	0.02495	0.00627
U_s+I_s	35.2	-64.49	0.00820	0.00205
	63.0	67.56	0.02692	0.00749
	117.7	43.87	0.02677	0.00751
	238.2	38.02	0.03271	0.00906
	383.6	0.80	0.03231	0.00892
U_s + $T_{in}Wat$	104.3	-387.38	0.00516	0.00126
	134.8	30.59	0.01639	0.00401
	173.1	17.45	0.01640	0.00408
	262.2	31.77	0.02959	0.00710
	335.8	13.16	0.02921	0.00700
U_s +	10.4	51.40	0.02166	0.00623
	27.9	85.63	0.03287	0.00989

$P_{out}H_2$	94.5	54.94	0.03268	0.00986
	202.5	47.31	0.03828	0.01116
	344.5	10.91	0.03783	0.01099

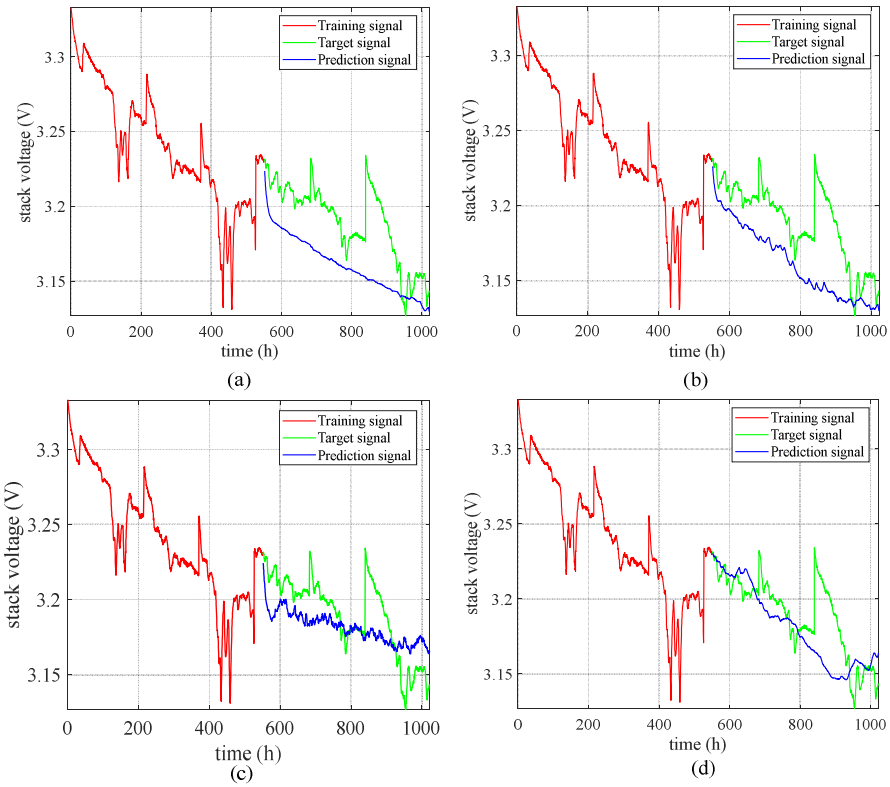

Fig. 15. The RUL prediction of FC2 based on 3-input ESN: (a) stack voltage (U_s), inlet temperature of H_2 ($T_{in}H_2$) and inlet pressure of H_2 ($P_{in}H_2$). (b) stack voltage (U_s), outlet temperature of H_2 ($T_{out}H_2$) and outlet temperature of air ($T_{out}Air$). (c) stack voltage (U_s), inlet temperature of air ($T_{in}Air$) and outlet pressure of air ($P_{out}Air$). (d) stack voltage (U_s), inlet temperature of water ($T_{in}Wat$), and inlet pressure of H_2 ($P_{in}H_2$).

TABLE Ⅶ. PREDICTION RESULTS OF FC2 BASED ON 3-INPUT ESN

inputs	Prediction values (h)	$\%Er_{FT}$	RMSE	MAPE
U_s +$T_{in}H_2$ +$P_{in}H_2$	5.9	72.43	0.02594	0.00787
	18.2	90.63	0.03147	0.00959
	119.5	43.01	0.03122	0.00953
	220.1	42.73	0.03608	0.01052
	376.5	2.64	0.03564	0.01036
U_s +$T_{out}H_2$ +$T_{out}Air$	9.5	55.61	0.01677	0.00493
	66.0	66.01	0.02405	0.00705
	147.2	29.80	0.02404	0.00708
	232.1	39.60	0.03522	0.00974
	308.1	20.33	0.03487	0.00964
U_s +$T_{in}Air$ +$P_{out}Air$	6.0	71.96	0.02631	0.00799
	15.5	92.02	0.02048	0.00587
	234.6	-11.87	0.01985	0.00561
	500.0	-30.11	0.02042	0.00520
	500.0	-29.30	0.02024	0.00516
U_s +$T_{in}Wat$	114.7	-435.98	0.00593	0.00141
	148.1	23.74	0.01175	0.00300
	246.5	-17.55	0.01140	0.00288

+$P_{in}H_2$	309.2	19.54	0.02466	0.00554
	500.0	-29.30	0.02435	0.00548

D. Multi-Input Analysis

In order to test all possible combinations, the prediction results based on all the 2-input ESN of FC1 and FC2 are shown in table Ⅷ and table Ⅸ, respectively. The $RMSE_i$ (i =1, 2, …, 5) are the RMSE between the prediction time and the different failure times. In FC1, the $RMSE_5$ is the RMSE between 550.0 h to 904.5 h and the $RMSE_5$ in FC2 is the RMSE between 550.0 h to 936.7 h. Therefore, the $RMSE_5$ is used to quantify the prediction accuracy. The $RMSE_5$ of single-input ESN in FC1 and FC2 are 0.02710 and 0.03789, respectively. Results show that the $RMSE_5$ of randomly 2-input ESN is smaller than single-input ESN both in FC1 and FC2. The optimal combination in FC1 is the U_s with T_{in}Wat (improved 59.20 %) and the optimal combination in FC2 is the U_s with T_{out}Air (improved 34.15 %). All the other 3-input combinations are tested to verify the prediction accuracy. The results of FC1 and FC2 are shown in Table Ⅹ and Table Ⅺ, respectively. The numbers (from 9 to 19) in Table Ⅹ and Table Ⅺ represent the inputs (from I_s to $P_{in}H_2$) in Table Ⅷ and Table Ⅸ. Compared the results of 2-input ESN and 3-input ESN in both FC1 and FC2, some of the 3-input ESN have a better performance than 2-input ESN, but some combinations have worse performance instead. Even some 3-input ESN combinations are worse than single-input ESN.

In the results of 3-input ESN, “better” (in green) means the $RMSE_5$ is smaller than any 2-input combinations, “worse” (in purple) means the $RMSE_5$ is bigger than any 2-input combinations, and “middle” (in blue) means the $RMSE_5$ is in between of the 2 combinations of 2-input. For example, in table Ⅹ, the “U_s+10+11” is “better”, and the $RMSE_5$ of “U_s+10+11” (0.01216) is small than “U_s+10” (0.01294) or “U_s+11” (0.01380); the “U_s+9+12” is “middle”, and the $RMSE_5$ of “U_s+9+12” (0.01505) is bigger than “U_s+12” (0.01260) and small than “U_s+9” (0.01532); the “U_s+18+19” is “worse”, and the $RMSE_5$ of “U_s+18+19” (0.01027) is bigger than “U_s+18” (0.01236) and “U_s+19” (0.01168). There are 39 “better” combinations and 11 “middle” combinations in FC1 and the “U_s+13+14” has the best performance. There are 21 “better” combinations and 24 “middle” combinations in FC2 and the “U_s+12+17” has the best performance. Besides, when compared all the “better” combinations of 3-input to the 2-input ESN, there are 12 combinations in FC1 have a smaller $RMSE_5$ than the 2-input ESN of “U_s+T_{in}Wat”. Nevertheless, there are 3 combinations (“U_s+9+12”, “U_s+12+17”, and “U_s+14+19”) in FC2 could have a smaller $RMSE_5$ than the 2-input ESN of “U_s+T_{out}Air”. The results show that 3-input ESN has the potential ability to improve the performance than 2-input ESN, especially under the static condition. But when considering the interaction of input variables, the selection of inputs is a rewarding area for further study. Considering the prediction accuracy and the computational complexity, the 2-input ESN has a top priority in both FC1 and FC2.

TABLE Ⅷ. THE IMPROVEMENT RESULTS OF FC1 BASED ON 2-INPUT ESN

Inputs	$RMSE_5$	improvement (%)
U_s	0.02710	--
U_s+T_{in}Wat(14)	**0.01106**	**59.20**
U_s+$P_{in}H_2$(19)	0.01168	56.90
U_s+$P_{out}H_2$(18)	0.01236	54.37
U_s+T_{in}Air(12)	0.01260	53.51
U_s+P_{in}Air(16)	0.01265	53.31
U_s+$T_{in}H_2$(10)	0.01294	52.24
U_s+P_{out}Air(17)	0.01336	50.71
U_s+T_{out}Air(13)	0.01339	50.59
U_s+$T_{out}H_2$(11)	0.01380	49.08
U_s+T_{out}Wat(15)	0.01440	46.84
U_s+I_s(9)	0.01532	43.47

TABLE Ⅸ. THE IMPROVEMENT RESULTS OF FC2 BASED ON 2-INPUT ESN

Inputs	$RMSE_5$	improvement (%)

U_s	0.03789	--
U_s+T_{out}Air(13)	**0.02495**	**34.15**
U_s+T_{in}Wat(14)	0.02921	22.90
U_s+T_{in}Air(12)	0.03023	20.21
U_s+$T_{out}H_2$(11)	0.03039	19.79
U_s+I_s(9)	0.03231	14.74
U_s+$T_{in}H_2$(10)	0.03242	14.43
U_s+P_{out}Air(17)	0.03292	13.13
U_s+T_{out}Wat(15)	0.03587	5.34
U_s+$P_{in}H_2$(19)	0.03589	5.30
U_s+PinAIR(16)	0.03715	1.96
U_s+$P_{out}H_2$(18)	0.03783	0.16

TABLE Ⅹ. THE PREDICTION RESULTS BASED ON ALL 3-INPUT COMBINATIONS OF FC1

Inputs	$RMSE_5$	Inputs	$RMSE_5$	Inputs	$RMSE_5$	Inputs	$RMSE_5$	Inputs	$RMSE_5$
U_s+9+10	0.01179	U_s+10+12	0.01053	U_s+11+15	0.01231	U_s+12+19	0.01070	U_s+14+19	0.01020
U_s+9+11	0.01369	U_s+10+13	0.01158	U_s+11+16	0.01161	U_s+13+14	**0.00981**	U_s+15+16	0.01459
U_s+9+12	0.01505	U_s+10+14	0.01052	U_s+11+17	0.01227	U_s+13+15	0.01227	U_s+15+17	0.01461
U_s+9+13	0.01401	U_s+10+15	0.01155	U_s+11+18	0.01205	U_s+13+16	0.01221	U_s+15+18	0.01463
U_s+9+14	0.01119	U_s+10+16	0.01090	U_s+11+19	0.01120	U_s+13+17	0.01252	U_s+15+19	0.01374
U_s+9+15	0.01168	U_s+10+17	0.01149	U_s+12+13	0.01163	U_s+13+18	0.01242	U_s+16+17	0.01387
U_s+9+16	0.01187	U_s+10+18	0.01134	U_s+12+14	0.01120	U_s+13+19	0.01141	U_s+16+18	0.01166
U_s+9+17	0.01230	U_s+10+19	0.01051	U_s+12+15	0.01266	U_s+14+15	0.01142	U_s+16+19	0.01109
U_s+9+18	0.01193	U_s+11+12	0.01175	U_s+12+16	0.01100	U_s+14+16	0.01035	U_s+17+18	0.01210
U_s+9+19	0.01215	U_s+11+13	0.01075	U_s+12+17	0.01179	U_s+14+17	0.01068	U_s+17+19	0.01180
U_s+10+11	0.01216	U_s+11+14	0.01135	U_s+12+18	0.01125	U_s+14+18	0.01087	U_s+18+19	0.01027

TABLE Ⅺ. THE PREDICTION RESULTS BASED ON ALL 3-INPUT COMBINATIONS OF FC2

Inputs	$RMSE_5$	Inputs	$RMSE_5$	Inputs	$RMSE_5$	Inputs	$RMSE_5$	Inputs	$RMSE_5$
U_s+9+10	0.03104	U_s+10+12	0.02763	U_s+11+15	0.03620	U_s+12+19	0.03097	U_s+14+19	0.02435
U_s+9+11	0.03055	U_s+10+13	0.03467	U_s+11+16	0.03334	U_s+13+14	0.02912	U_s+15+16	0.03511
U_s+9+12	0.02371	U_s+10+14	0.03659	U_s+11+17	0.03037	U_s+13+15	0.03288	U_s+15+17	0.03261
U_s+9+13	0.02727	U_s+10+15	0.03661	U_s+11+18	0.03497	U_s+13+16	0.02782	U_s+15+18	0.03782
U_s+9+14	0.03248	U_s+10+16	0.03377	U_s+11+19	0.03457	U_s+13+17	0.02709	U_s+15+19	0.03675
U_s+9+15	0.03865	U_s+10+17	0.03055	U_s+12+13	0.02817	U_s+13+18	0.02911	U_s+16+17	0.03146
U_s+9+16	0.03555	U_s+10+18	0.03560	U_s+12+14	0.03250	U_s+13+19	0.02765	U_s+16+18	0.03498
U_s+9+17	0.02954	U_s+10+19	0.03564	U_s+12+15	0.03202	U_s+14+15	0.03558	U_s+16+19	0.03295
U_s+9+18	0.03272	U_s+11+12	0.02523	U_s+12+16	0.02778	U_s+14+16	0.02946	U_s+17+18	0.02985
U_s+9+19	0.02982	U_s+11+13	0.03487	U_s+12+17	**0.02024**	U_s+14+17	0.02904	U_s+17+19	0.02831
U_s+10+11	0.02674	U_s+11+14	0.03625	U_s+12+18	0.03119	U_s+14+18	0.02825	U_s+18+19	0.03775

V. CONCLUSION

Echo state network (ESN) is an interesting and promising data-driven tool to implement the RUL prediction for the PEMFC systems. Unlike the model-based and hybrid RUL prediction methods, the mathematical model is unnecessary for the ESN method and the degradation tendency can be directly extracted from a large amount of historical data. As the improvement structure of recurrent neural network, the ESN has the advantages of low computational complexity and fast convergence rate. Therefore, the ESN based data-driven method has a rapid response on lifespan prediction and the results are meaningful for the control policy to extend the lifespan of fuel cell. In order to improve the prediction performance, a multi-input and multi-output ESN (MIMO-ESN) method is proposed in this work. Besides the commonly used stack voltage, the operating parameters, such as stack current, stack temperature and the pressures of the reactants are also utilized as the inputs of ESN. The single-input, 2-input, and 3-input ESN are designed and tested on the datasets which were acquired from the test bench for more than 1000 hours' duration. The feasibility and effectiveness of the proposed MIMO-ESN are verified under both static and quasi-dynamic operation conditions. Experimental results show that MIMO-ESN has the capability to improve the prediction accuracy, especially the 2-input ESN with an improvement of 59.20 % (static condition) and 34.15 % (quasi-dynamic condition) in terms of $RMSE_5$ respectively compared with the traditionally used SISO-ESN. In the next-step study, novel health indicators and multi-step prediction approaches under different operating profiles will be further explored. Meanwhile, the implementation and verification of the MIMO-ESN algorithm in the actual vehicle applications will be further investigated.

ACKNOWLEDGMENT

This work has been supported by the European Commission H2020 grant PANDA (H2020-LC-GV-2018), EU Grant agreement No: 824256 and the ANR project BIPHOPROC_2 (ANR-14-OHRI-0018).

REFERENCES

[1] X. Luo, J. Wang, M. Dooner, and J. Clarke, "Overview of current development in electrical energy storage technologies and the application potential in power system operation," Applied Energy, vol. 137, pp. 511-536, Jan. 2015.

[2] A. Simons and C. Bauer, "A life-cycle perspective on automotive fuel cells," Applied Energy, vol. 157, pp. 884-896, Nov. 2015.

[3] Y. Wang, K. S. Chen, J. Mishler, S. C. Cho, and X. C. Adroher, "A review of polymer electrolyte membrane fuel cells: technology, applications, and needs on fundamental research," Applied Energy, vol. 88, pp. 981-1007, Apr. 2011.

[4] Y. Yan, Q. Li, W. Chen, B. Su, J. Liu, and L. Ma, "Optimal energy management and control in multimode equivalent energy consumption of fuel cell/supercapacitor of hybrid electric tram," IEEE Transactions on Industrial Electronics, vol. 66, pp. 6065-6076, 2019.

[5] H. Liu, J. Chen, D. Hissel, and H. Su, "Remaining useful life estimation for proton exchange membrane fuel cells using a hybrid method," Applied Energy, vol. 237, pp. 910-919, Mar. 2019.

[6] U.S. Department of Energy (DOE). Fuel Cells, 2016 (Update May 2017). https://www.energy.gov/sites/prod/files/2017/05 /f34/fcto_myrdd_ fuel_cells.pdf

[7] ISO13381-1. Condition monitoring and diagnostics of machines - prognostics - part1: general guidelines. International Standard, ISO; 2004.

[8] R. Gouriveau, M. Hilairet, D. Hissel, S. Jemei, M. Jouin, E. Lechartier, S. Morando, E. Pahon, M. C. Péra, and N. Zerhouni, "IEEE phm 2014 data challenge: oultine, experiments, scoring of results, winners, " tech. rep., IEEE 2014 PHM Challenge, 2014.

[9] M. Jouin, M. Bressel, S. Morando, R. Gouriveau, D. Hissel, M. C. Péra, et al., "Estimating the end-of-life of PEM fuel cells: guidelines and metrics," Applied Energy, vol. 177, pp. 87-97, Sep. 2016.

[10] J. Lee, F. Wu, W. Zhao, M. Ghaffari, L. Liao, and D. Siegel, "Prognostics and health management design for rotary machinery systems-reviews, methodology and applications," Mechanical Systems and Signal Processing, vol. 42, pp. 314-334, Jan. 2014.

[11] Z. Hua, Z. Zheng, F. Gao, M. C. Péra. "Challenges of the remaining useful life prediction for proton exchange membrane fuel cells " in IECON 2019 - 45th Annual Conference of the IEEE Industrial Electronics Society, pp. 6382-6387, 2019.

[12] E. Lechartier, E. Laffly, M.-C. Péra, R. Gouriveau, D. Hissel, and N. Zerhouni, "Proton exchange membrane fuel cell behavioral model suitable for prognostics," International Journal of Hydrogen Energy, vol. 40, pp. 8384-8397, Jul. 2015.

[13] C. Robin, M. Gerard, A. A. Franco, and P. Schott, "Multi-scale coupling between two dynamical models for PEMFC aging prediction," International Journal of Hydrogen Energy, vol. 38, pp. 4675-4688, Apr. 2013.

[14] P. Pei and H. Chen, "Main factors affecting the lifetime of proton exchange membrane fuel cells in vehicle applications: A review," Applied Energy, vol. 125, pp. 60-75, Jul. 2014.

[15] X. Z. P. Pisu, "An unscented kalman filter based approach for the health-monitoring and prognostics of a electrolyte membrane fuel cell polymer," in 2012 Annual Conference of Prognostics and Health Management Society, pp. 1-9, 2012.

[16] M. Bressel, M. Hilairet, D. Hissel, and B. O. Bouamama, "Extended kalman filter for prognostic of proton exchange membrane fuel cell," Applied Energy, vol. 164, pp. 220-227, Feb. 2016.

[17] M. Jouin, R. Gouriveau, D. Hissel, M.-C. Péra, and N. Zerhouni, "Prognostics of PEM fuel cell in a particle filtering framework," International Journal of Hydrogen Energy, vol. 39, pp. 481-494, Jan. 2014.

[18] J. K. Kimotho, T. Meyer, and W. Sextro, "PEM fuel cell prognostics using particle filter with model parameter adaptation," in 2014 International Conference on Prognostics and Health Management, pp. 1-6, 2014.

[19] Y. Wu, E. Breaz, F. Gao, D. Paire, and A. Miraoui, "Nonlinear performance degradation prediction of proton exchange membrane fuel cells using relevance vector machine," IEEE Transactions on Energy Conversion, vol. 31, pp. 1570-1582, Dec. 2016.

[20] Y. Wu, E. Breaz, F. Gao, and A. Miraoui, "A modified relevance vectormachine for PEM fuel-cell stack aging prediction," IEEE Transactions on Industry Applications, vol. 52, pp. 2573-2581, May./Jun. 2016.

[21] R. E. Silva, R. Gouriveau, S. Jemeï, D. Hissel, L. Boulon, K. Agbossou, et al., "Proton exchange membrane fuel cell degradation prediction based on adaptive neuro-fuzzy inference systems," International Journal of Hydrogen Energy, vol. 39, pp. 11128-11144, Jul. 2014.

[22] K. Javed, R. Gouriveau, N. Zerhouni, D. Hissel, "Data-driven prognostics of proton exchange membrane fuel cell stack with constraint based summation-wavelet extreme learning machine," in 2016 International Conference on Fundamentals & Development of Fuel Cells, pp. 1-8, 2015.

[23] R. Ma, E. Breaz, C. Liu, H. Bai, P. Briois, and F. Gao, "Data-driven prognostics for pem fuel cell degradation by long short-term memory network," in 2018 IEEE Transportation Electrification Conference and Expo (ITEC), pp. 102-107, 2018.

[24] J. Liu, Q. Li, W. Chen, Y. Yan, Y. Qiu, and T. Cao, "Remaining useful life prediction of PEMFC based on long short-term memory recurrent neural networks," International Journal of Hydrogen Energy, vol. 44, pp. 5470-5480, Feb. 2019.

[25] R. Ma, T. Yang, E. Breaz, Z. Li, P. Briois, and F. Gao, "Data-driven proton exchange membrane fuel cell degradation predication through deep learning method," Applied Energy, vol. 231, pp. 102-115, Dec. 2018.

[26] J. Liu, A. Saxena, K. Goebel, B. Saha, W. Wang, "An adaptive recurrent neural network for remaining useful life prediction of lithium-ion batteries," in the Annual Conference of the Prognostics and Health Management Society, pp. 1-9, 2010.

[27] F. O. Heimes, "Recurrent neural networks for remaining useful life estimation," in 2008 International Conference on Prognostics and Health Management, pp. 1-6, 2008.

[28] H. Jaeger, "The 'echo state' approach to analysing and training recurrent neural networks-with an erratum note," Fraunhofer Institute for Autonomous Intelligent Systems, 2010.

[29] H. Jaeger, "Tutorial on training recurrent neural networks, covering BPTT, RURL, EKF and the 'Echo State Network' approach," Technical report GMD-German National Research Center for Information Technology, 2002.

[30] W. Maass, T. Natschläger, and H. Markram. "Real-time computing without stable states: a new framework for neural computation based on perturbations," Neural computation, vol. 14, pp. 2531-2560, 2002.

[31] J. J. Steil. "Backpropagation-Decorrelation: online recurrentlearning with O(N) complexity," in the IEEE International Joint Conference on Neural Networks, pp. 843-848, 2004.

[32] Z. Zheng, M. C. Péra, D. Hissel, L. Larger, N. Y. Steiner, and S. Jemei, "Fault diagnosis of PEMFC systems in the model space using reservoir computing," in 2018 IEEE Vehicle Power and Propulsion Conference (VPPC), pp. 1-5, 2018.

[33] Z. Zheng, S. Morando, M. C. Péra, D. Hissel, L. Larger, R. Martinenghi, A. B. Fuentes. "Brain-inspired computational paradigm dedicated to fault diagnosis of PEM fuel cell stack," International Journal of Hydrogen Energy, vol. 42, pp. 5410-5425, Feb. 2017.

[34] S. Morando, M. C. Péra, N. Y. Steiner, S. Jemei, D. Hissel, and L. Larger, "Fuel cells fault diagnosis under dynamic load profile using reservoir computing," in 2016 IEEE Vehicle Power and Propulsion Conference (VPPC), pp. 1-6, 2016.

[35] S. Morando, M. C. Péra, N. Y. Steiner, S. Jemei, D. Hissel, and L. Larger, "Reservoir computing optimisation for PEM fuel cell fault diagnostic," in 2017 IEEE Vehicle Power and Propulsion Conference (VPPC), pp. 1-7, 2017.

[36] S. Morando, S. Jemei, R. Gouriveau, N. Zerhouni, and D. Hissel, "Fuel cells prognostics using echo state network," in IECON 2013 - 39th Annual Conference of the IEEE Industrial Electronics Society, pp. 1632-1637, 2013.

[37] S. Morando, S. Jemei, R. Gouriveau, N. Zerhouni, and D. Hissel, "Fuel cells remaining useful lifetime forecasting using echo state network," in 2014 IEEE Vehicle Power and Propulsion Conference (VPPC), pp. 1-6, 2014.

[38] S. Morando, S. Jemei, D. Hissel, R. Gouriveau, and N. Zerhouni, "Proton exchange membrane fuel cell ageing forecasting algorithm based on echo state network," International Journal of Hydrogen Energy, vol. 42, pp. 1472-1480, Jan. 2017.

[39] R. Mezzi, S. Morando, N. Y. Steiner, M. C. Péra, D. Hissel, and L. Larger, "Multi-reservoir echo state network for proton exchange membrane fuel cell remaining useful life prediction," in IECON 2018 - 44th Annual Conference of the IEEE Industrial Electronics Society, pp. 1872-1877, 2018.

[40] Z. Li, S. Jemei, R. Gouriveau, D. Hissel, and N. Zerhouni, "Remaining useful life estimation for PEMFC in dynamic operating conditions," in 2016 IEEE Vehicle Power and Propulsion Conference (VPPC), pp. 1-6, 2016.

[41] Z. Li, Z. Zheng, and R. Outbib, "Adaptive prognostic of fuel cells by implementing ensemble Echo State Networks in time varying model space, " IEEE Transactions on Industrial Electronics, vol. 67, pp. 379-389, 2020.

[42] M. Lukoševičius, "A practical guide to applying echo state networks. neural networks: tricks of the trade, " Neural Networks: Tricks of the Trade, pp. 659-686, 2012.

[43] Z. Hua, D. Zhao, M. Dou, L. Yan, and H. Zhang, "Modeling and control of brushless dc motor for compressor driving," in 2017 IEEE Energy Conversion Congress and Exposition (ECCE), pp. 5553-5556, 2017.

[44] A. Hochstein, H. I. Ahn, Y. T. Leung, and M. Denesuk, "Switching vector autoregressive models with higher-order regime dynamics," in 2014 International Conference on Prognostics and Health Management, pp. 1-10, 2014.